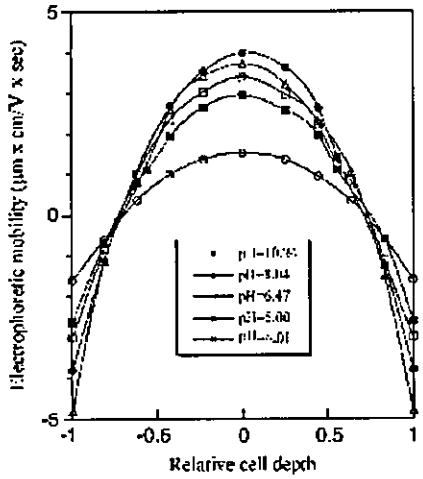


Fig. 3 Apparent flow velocity profile of standard latex samples at various pH values ($1 \times 10^{-3}$ M KCl, 25°C).

in which an electrical field arises in colloidal suspension when a sound wave passes through the dispersion (i.e., ultrasonic vibration causes the difference in movement between charged core particles and countercharges around them, which induces oscillating dipole moments and hence the potential drop in the sample cell);[9] and 2) electrokinetic sonic amplitude (ESA), the reciprocal effect of the above phenomena, in which an alternating electrical field is applied to a suspension and a sound wave arises as a result of the inertia of the particles, caused by their time-alternating electrophoresis (i.e., high-frequency electrical waves cause a difference in movement between the core particles and the countercharges, which generates an ultrasonic waves in the sample cell).[10,11]

A very important advantage of these electroacoustical techniques is their ability to provide accurate measurements of the ζ-potential in concentrated colloid systems. In this section, two of the typical data obtained by these methods are shown.

## Surface Characterization of Concentrated Latex Suspensions

In this section, the CVP technique is demonstrated for zeta potential measurements of concentrated suspensions of latex particles with different surface groups.[12] Three types of polystyrene lattices with different surface groups were synthesized in emulsifier-free systems. The usual polystyrene (PSt) lattices were prepared by the method of Kotera et al.,[13] and the two others (PSm and PStn) were synthesized by incorporating small amounts of ionic

Table 2 Characterization of colloid particles

| Sample | Diameter (nm) | Surface charge density (μC/cm²) Strong acid | Weak acid | Total |
|---|---|---|---|---|
| PSt | 480 | 5.3 | 2.5 | 7.8 |
| PStn | 610 | 18 | 0 | 18 |
| PStm | 530 | 5 | 33 | 38 |

comonomer, methacrylic acid, and sodium polyvinylphenylsulfonate (NaSS) into a polystyrene chain, respectively, as in Juang and Krieger.[14] To increase the particle size, PStn was prepared in a system with $1 \times 10^{-4}$ mol/dm³ $MgSO_4$. These latex samples were sufficiently dialyzed with distilled water and were then brought into contact with an ion exchange resin to remove ionic impurities. The samples were all composed of highly monodispersed spherical particles with $D_w/D_n = 1.02$, and the surface charge densities of the latex particles were measured by potentiometric and conductometric titration, as in Van den Hul and Vanderhoff.[15] The characterization data of all the samples are summarized in Table 2.

To compare the CVP with the conventional electrokinetic technique, first, the zeta potential of each sample in a dilute state was determined in a $1 \times 10^{-3}$ mol/dm³ KCl solution at different pH values using the microelectrophoretic technique. The resulting data for four samples are shown in Fig. 4. The ζ-potential of the latex samples, especially the PStn sample, appears to be essentially independent of the medium pH. The zeta potential of PSt increases gradually from acidic to neutral pH. This behavior is probably dependent on the existence of carboxyl groups on the surface (with $pK_a$ values between

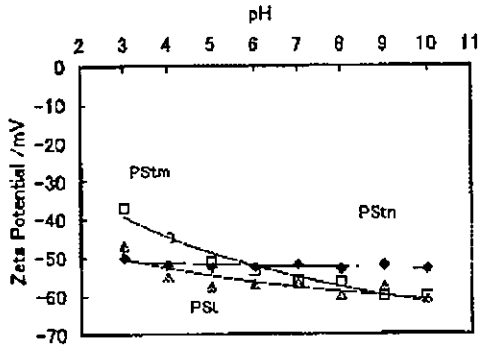


Fig. 4 pH dependence of zeta potential in dilute state measured by the microelectrophoretic technique in $1 \times 10^{-3}$ mol/dm³ KCl at 25°C.

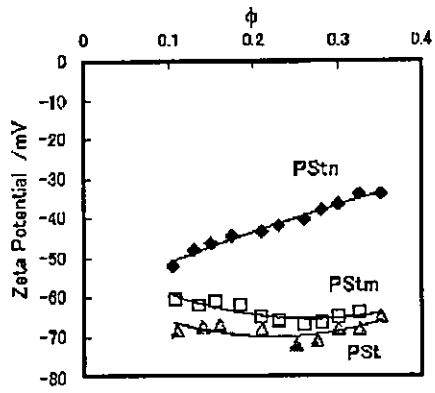


Fig. 5 Concentration dependence of zeta potential for polystyrene latex suspensions in $1 \times 10^{-3}$ mol/dm$^3$ KCl at 25°C and pH 5.

about 4 and 5), which are produced by the hydrolysis and subsequent oxidation of the $OSO_3^-$ groups that come from the radical fragments used as an initiator ($K_2S_2O_8$).[16–18]

The CVP measurements of polystyrene lattices give reliable data only in high-volume fraction ($\phi$) systems above $\phi$=0.1 because the density of the latex particles is small ($\rho_2$=1.05 g/cm$^3$) and significant differences of CVP against the background signal can be detected only at high concentration ranges. Figs. 5 and 6 are graphs of the zeta potentials determined by CVP measurements for three kinds of polystyrene lattices at pH 5 and 9, as a function of the $\phi$ value of each latex. It is apparent that the zeta potentials for PSt and PStm at pH 5 and for PSt at pH 9 have nearly constant values over the entire concentration range of particles, and that the cell model theory is nearly

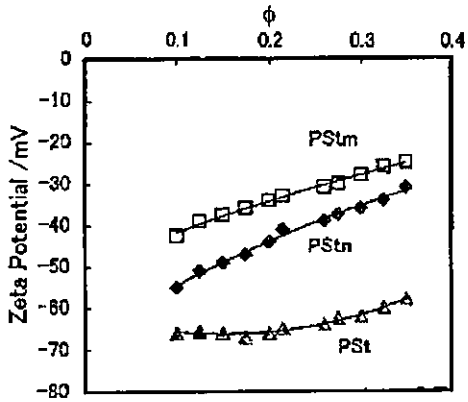


Fig. 6 Concentration dependence of zeta potential for polystyrene latex suspensions in $1 \times 10^{-3}$ mol/dm$^3$ KCl at 25°C and pH 9.

valid for those systems. However, the zeta potentials for PStn at pH 5 and for PStn and PStm at both pH values decrease strongly as the particle concentrations increase. Furthermore, it was found that those of PStm at pH 9 are lower than those at pH 5, which is opposite in tendency to those in Fig. 4, determined directly in dilute states by the microelectrophoretic technique. It is thought, from a comparison with Table 2, that this abnormal behavior of the $\zeta$-potential is related to the high surface charge densities of the latex samples (i.e., PStn has many sulfonate groups on the surface brought about by the NaSS component), which dissociate completely under both pH conditions, and PStm becomes covered with thick carboxyl layers coming from the MA molecules, which gradually dissociate as the pH increases. These high surface charge densities bring about an expansion of the surface layer and may cause a double-layer overlapping at moderate particle concentrations, which results in restrictions for the prerequisite of the cell model of Levine et al.[19]

To understand the abnormal behavior of the CVP and $\zeta$-potential that appeared in the latex suspensions, including the particles with high surface charge densities, the concentration dependence of conductivity was measured in the respective systems. The concentration dependence of the conductivity depends largely on the surface nature of the particles.[12] The conductivity of polystyrene latex systems increases as the particle concentration increases. This tendency is especially remarkable in the PStn systems at pH 5 and 9 and in the PStm system at pH 9. From a comparison with the results of the CVP, it was realized that this increasing tendency of the conductivity is closely related to the abnormal behavior of the CVP. This is explained as follows. On the highly charged surfaces of PStn or PStm at pH 9, a polyelectrolyte-like ("hairy") layer is present. These layers overlap each other in this concentrated state, allowing electrical conduction through the hairy layer; thus the hairy layer results in interparticle surface conductance. The degree of interparticle surface conduction is affected by the particle concentration and the thickness of the hairy layer, which in turn depend on the surface charge density of the particle and the pH of the medium.

## Application of Electrokinetic Sonic Amplitude Technique in the Ceramic Industry

The concept of colloidal suspension processing has been successfully applied to the field of structural ceramic where inherent properties of dense suspension are used to transform a fluid suspension to a stiff gel. During colloidal processing, the state of dispersion has a significant influence on the casting behavior and the resulting green body properties. The good dispersion of particles

gives optimum packing state (high green density), which influences the sinterability of the ceramic body and hence the physical and chemical properties of the final product. At present, fine-grained and uniform microstructures are desirable for most ceramic applications in producing strong and reliable structural parts.

Traditionally in the ceramic industry, polyelectrolytes have been utilized to prevent the flocculation of particles. Because of the charged nature of the polyelectrolyte, they impart stability to the particles via an electrosteric mechanism. Hence the adsorption of these charged molecules onto a particle surface will alter the surface charge and hence the zeta potential. Thus using electroacoustics, it is possible to follow the changes in the zeta potential with increasing amounts of polyelectrolyte. This is extremely useful in determining the optimum amount of polyelectrolyte required to stabilize the particles under different conditions.

Fig. 7 shows how the zeta potential of an alumina suspension (background electrolyte, 10 mM KCl) can be altered by the addition of three commercially available polyelectrolytes.[20] Initially, the zeta potential of the suspension is such that the suspension becomes more stable. The trend for all dispersants is very similar in that, initially, the zeta potential changes strongly with small amounts of dispersants and then after a certain concentration, the zeta potential begins to plateau out as no more dispersant is adsorbed on the surface. However, each dispersant imparts a different final zeta potential and requires a different amount of dispersants to cover the particles. Of these, Poly-CA imparts the greatest final zeta potential, so this would be an excellent dispersant for the alumina. However, it must be noted that the likely stabilization mechanism for polyelectrolyte dispersants is electrosteric stabilization. Therefore there may well be a steric contribution to the stabilization mechanism depending on how the dispersant adsorbs. Poly-CE64 imparts a final zeta potential of −45 mV and requires approximately twice as much dispersant to do so, making it a poor candidate in comparison. The zeta potential from the suspension stabilized with Poly-PC 33 does not appear to level out, and further data points would be required to determine the optimum amount.

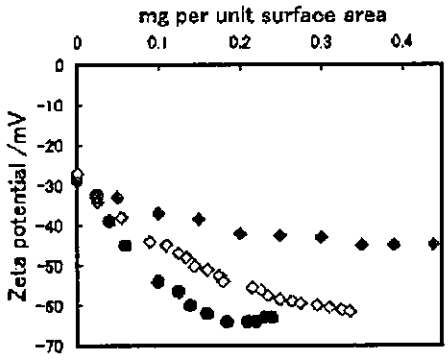


Fig. 7 Effect of three commercial dispersants on alumina suspension in $1 \times 10^{-4}$ mol/dm$^3$ KCl: (●) Poly-CA; (◇) Poly-PC33; (◆) Poly-CE64.

## ELECTROKINETIC MEASUREMENTS IN SYNTHESIS OF COMPOSITE PARTICLES

There is a variety of methods currently used to fabricate a wide range of stable, composite, and coating particles of various compositions. These include heterocoagulation,[21] seed polymerization,[22] emulsion/phase separation,[23] sacrificial core techniques,[24] and so on. The notion of adsorbing particles onto solid substrates in a layer-by-layer manner was introduced by Iler[25] in the mid-1960s. Decher and Hong[26] extended Iler's work to a combination of linear polycations and polyanions in the early 1990s. Decher[27] later adapted the layer-by-layer technique to include inorganic nanoparticles, biomolecules, clays, and dyes in polyelectrolyte multilayer assemblies. Very recently, Caruso and Mohwald[28] and Caruso et al.[29] reported very interesting results, which included a detailed investigation of the stepwise formation of the silica–nanoparticle/polymer multilayer templating of some latex particles. In this chapter, we demonstrate how we can utilize electrophoretic measurements in synthesis and coating processes of composite particles.

### Heterocoagulation Behavior of Polymer Lattices with Spherical Silica

Gherardi and Matijevic[30] have investigated various behaviors of mixed colloid particles obtained by mixing differently preformed particles. They showed that the nature of a mixing system depends on the conditions of preparations, and concluded that the most important parameter in controlling the morphology of composite particles is the surface charge of the component particles, especially the contrast between surface charges of the two component particles. A stable system consisting of a regular composite particle could be prepared only in a medium controlled at a definite pH, where the two components are charged with opposite signs. Typical results



MARCEL DEKKER, INC.
270 Madison Avenue, New York, New York 10016

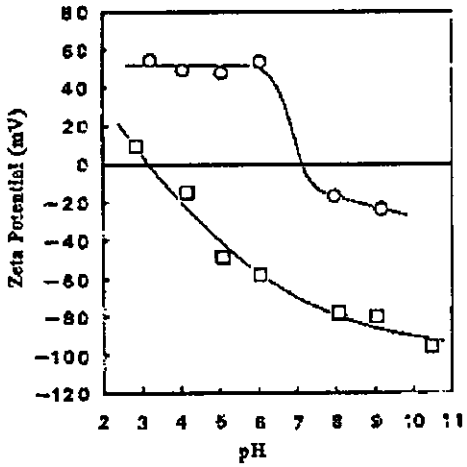


Fig. 8 ζ-Potentials of silica (□) and latex particles (○) as a function of pH at $5 \times 10^{-3}$ mol/dm$^3$ KCl.

of the electrophoretic mobility for the single silica and the latex suspension are shown in Fig. 8.

The next important parameter to control morphology is the particle size ratio of the component particles when they are mixed in the vessel. Fig. 9 shows schematic pictures of the morphology of heterocoagulates of different silica particles and amphoteric lattices. Fig. 10 shows an optical micrograph of the real heterocoagulate generated from different silica samples and amphoteric latex systems, where the other conditions (e.g., the particle number ratio, $N_{silica}/N_{latex}=1/300$; medium pH 5.6) have been kept constant. The microscope used for

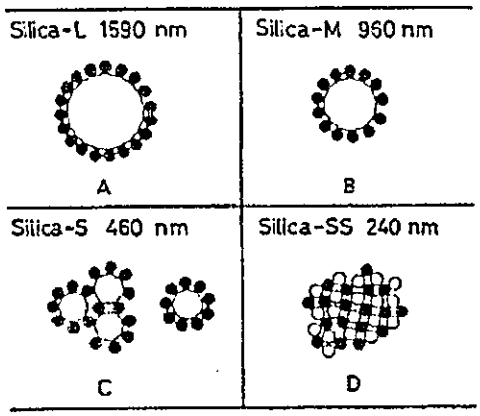


Fig. 9 Schematic pictures showing the morphology of heterocoagulate particles formed from different silica samples.

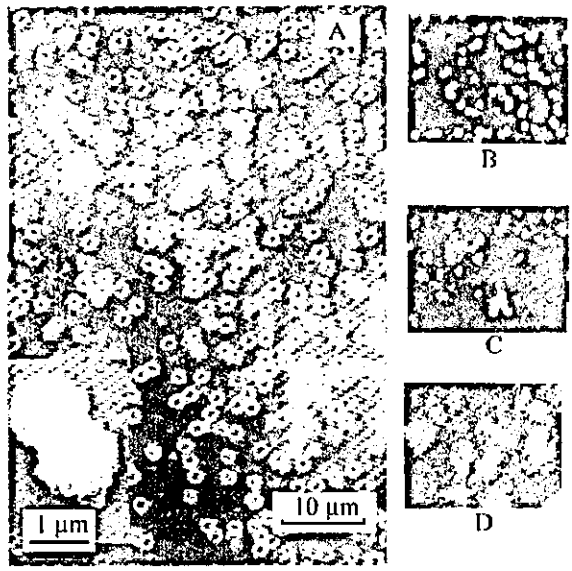


Fig. 10 Optical micrograph showing the heterocoagulates prepared from different silica samples: (A) Silica-L; (B) Silica-M; (C) Silica-S: (D) Silica-SS.

observations was a lateral-type metallurgical microscope (Axio Mart, Carl Zeiss, Germany). It may be seen that at a particle size ratio ($r=D_{silica}/D_{latex}$) higher than 3, the suspension is composed of uniform heterocoagulate particles and each heterocoagulate undergoes Brownian motion as an isolated unit. The insert of Fig. 10A shows a scanning electron micrograph of the heterocoagulate. It

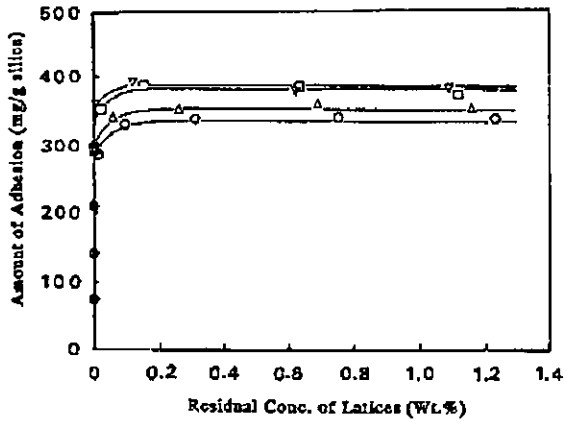


Fig. 11 Adhesion isotherms of amphoteric lattices onto Silica-L at various $K_2SO_4$ concentrations: (▽) $1.46 \times 10^{-2}$ M; (□) $1.46 \times 10^{-3}$ M; (△) $1.46 \times 10^{-4}$ M; (○) 0 M.

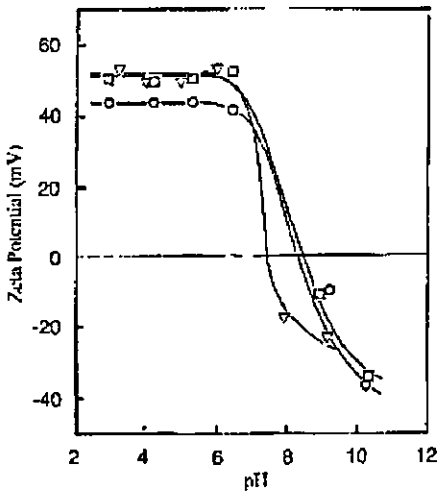


Fig. 12 $\zeta$-Potentials vs. pH curves for heterocoagulate particles prepared at different electrolytes: ($\nabla$) heterocoagulates prepared at $2.48 \times 10^{-1}$ M $MgCl_2$; (O) heterocoagulates prepared at $1 \times 10^{-5}$ M KCl; ($\square$) amphoteric lattices.

is apparent that the heterocoagulate takes a raspberry shape with one silica particle in the core. In contrast to this, the heterocoagulates generated at a particle size ratio lower than $r$=3 (Fig. 10C and D) are composed of large, irregular aggregates, and regular coagulates were hardly formed at any medium pH and particle number ratio investigated.[31,32]

It is interesting to analyze the different heterocoagulation behaviors from the concept of the adhesion isotherm for the amphoteric lattices on the silica particles. Fig. 11 shows some typical isotherms for the lattices on Silica-L at various $K_2SO_4$ concentrations, where all the systems were controlled at pH 5.2. It is evident that the isotherms are all well defined and of very high affinity type, and the plateau value increases with increasing $K_2SO_4$ concentration within the range from $10^{-5}$ to $10^{-2}$ mol/dm$^3$. This means that in this concentration range, adhesion proceeds in a way characteristic of monolayer adhesion. This may be because of the strong blocking effect of adhering particles. However, in $K_2SO_4$ aqueous solutions more concentrated than $2 \times 10^{-2}$ mol/dm$^3$, no reproducible isotherm could be obtained under any conditions tested, and only some irregular aggregates were generated in the course of the experiment.[31] In Fig. 12, the $\zeta$-potentials of the heterocoagulates prepared at different electrolyte concentrations, as well as the data on the amphoteric lattices, are presented as a function of the medium pH. As may be seen, a reversal of charge is observed in all samples, and the IEP in the heterocoagulated systems

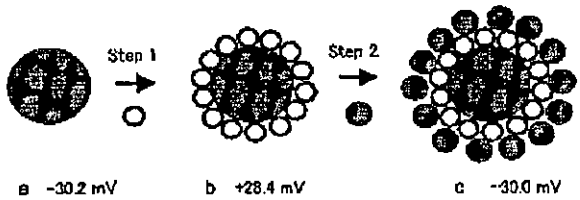


Fig. 13 Schematic showing the process of synthesizing multilayer composite particles: (a) core silica; (b) PC vesicle/silica composite particle; (c) silica/PC vesicle/silica composite particle.

occurs at about pH 8, which is not so different from the IEP of the single lattices. Moreover, the fact that the limiting net positive $\zeta$-potential attained at $3 < pH < 6$ increases with increasing electrolyte concentration is also in line with the increase in latex adhesion with increasing electrolyte concentration.

## Multilayer Composite Particles Comprising Silica/Vesicle/Silica Particles

Composite particles, including vesicle particles, are an important topic in application fields. Composite particles can be used frequently in the biomedical field for diagnostic purposes and for treatment medicine. Here, we describe one example of such systems,[33] that is, PC vesicles, which are typical biocolloid systems and are introduced into composites as a one-component particle.

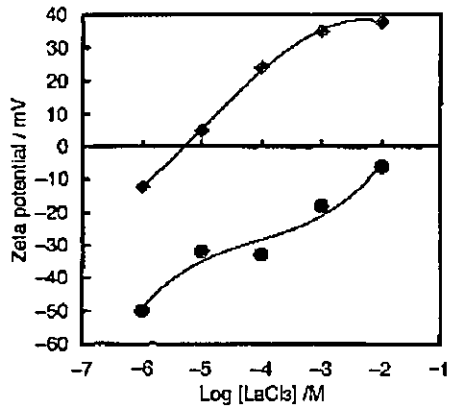


Fig. 14 $\zeta$-Potentials vs. the concentration of $LaCl_3$: (◆) PC vesicles; (●) silica particles.

The silica/PC vesicle/silica multilayer composite particles were prepared by the alternate adsorption of PC vesicles and small silica particles on the large silica particles with negative charges (Fig. 13). In this study, electrostatic attraction is taken into account as the driving force. It is important that the silica and the vesicle surfaces bear opposite charges to be effective. We can control the surface charges of the vesicle and silica particles by adjusting the concentration of $LaCl_3$. In Fig. 14, the $\zeta$-potentials of PC vesicles and silica particles are shown as a function of $LaCl_3$ concentration. The $\zeta$-potential of PC vesicles decreases with increasing $LaCl_3$ concentration, and becomes positive over a certain concentration of $LaCl_3$. This is because of the binding effect of $La^{3+}$ ions to the phospholipids head group.[34] However, for silica dispersions, the $\zeta$-potential remained negative over the $10^{-6}$–$10^{-2}$ M concentration range of $LaCl_3$. Thus at $10^{-4}$ M $LaCl_3$, the $\zeta$-potentials of the silica and PC vesicles were $-30$ and $+32$ mV, respectively. It is assumed that a strong electrostatic attraction will occur between the vesicles and the silica particles. Therefore we selected $10^{-4}$ M $LaCl_3$ as the heterocoagulation condition.

After mixing the PC vesicles with the core silica dispersion, the free vesicles were removed from the dispersion and the $\zeta$-potentials of the composite particles generated were measured. The value was determined to be +28 mV. The positive $\zeta$-potential indicates that the PC vesicles are adsorbed on the silica surface because the surface of the PC vesicles binds with $La^{3+}$ ions.

For the PC vesicle adsorption state on the silica surface, there are two possible states: 1) as a vesicle particle layer, or 2) as a lipid molecular bilayer. To clarify the adsorption state of the vesicles, as the next stage, the adsorption amounts of PC on the silica surface have been measured. In Fig. 15, the results are shown as a function of the PC concentration. Adsorption amounts are expressed by the number of phospholipids molecules adsorbed per square meter of silica surface. The solid line represents a theoretical curve for the adsorption amount of the single bilayer model, assuming the area per PC molecule equals 0.7 $nm^2$. The dotted line shows a theoretical curve for the adsorption of a single vesicle layer model, assuming that the vesicles are of uniform size and have a unilamellar spherical shape. The saturated adsorption amounts in the experiments are located near the value for the latter, but over it. This is because of the existence of some multilamellar PC vesicles in the sample (i.e., the existence of multilamellar PC vesicles will induce a large number of PC molecules than the value of unilamellar vesicles). Thus we can expect that the PC vesicles will be adsorbed on the silica surface as a unilamellar vesicle layer (i.e., the composite particles have been generated as shown in Fig. 13b). Furthermore, we then separated the PC vesicle/silica composites from the free PC vesicles by the ultra-filtration method (with a polycarbonate membrane filter, pore size 1.0 μm), and determined the mean size of the composite particles by the dynamic light scattering (DLS) method. The diameter of the composite particles is 1.93 μm, and this value is close to 1.9 μm, which was calculated by the single particle layer model. This result means that the PV vesicles will be adsorbed on silica particles as the same spherical particle size.

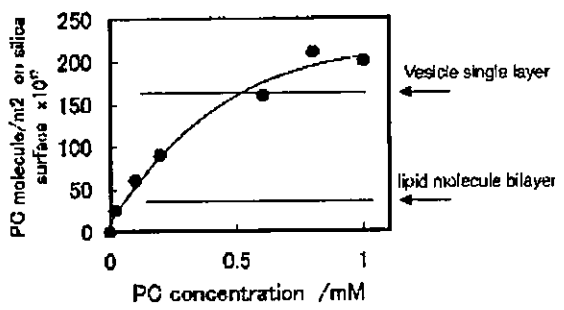


Fig. 15 Adsorption amount for PC on core silica surface in $10^{-4}$ M $LaCl_3$ at 25°C.

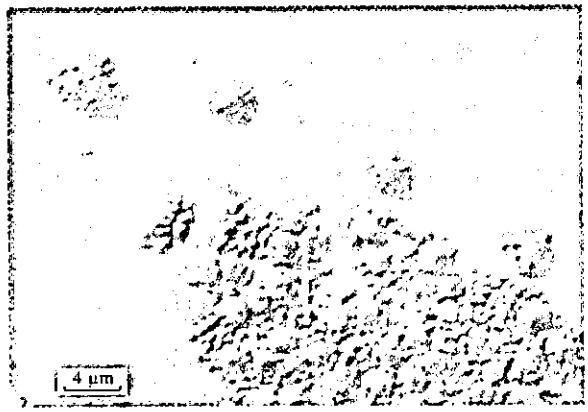


Fig. 16 Optical micrograph of silica/PC vesicles/silica composite particles. (*View this art in color at www.dekker.com.*)

In the second stage of composite formation, we mixed the PC vesicle/silica composite particles with a small silica ($2a$=0.5 μm) dispersion under the same $10^{-4}$ M $LaCl_3$ solution. The $\zeta$-potentials of the products reversed from positive (+28.4 mV) to negative ($-30$ mV) again, which indicates that the small silica particles (with negative charges) were adsorbed on the surface of the positively charged composite particles (Fig. 13c).

The direct observation of the multilayer formation of composite particles is provided by a special optical microscopy technique. In Fig. 16, the composite particles of the silica/PC vesicle/core silica in the $10^{-4}$ M $LaCl_3$ solution are shown. We cannot clearly see the image of the PC vesicles on the silica because the PC vesicle has a large water core and a thin lipid bilayer (about 5 nm). Therefore the total refractive indices of the PC vesicle are close to those of water. However, the formation of the silica/PC vesicle/silica composite particles is indicated clearly in Fig. 16; the small silica particles are adsorbed on the spherical surface of the PC vesicle/core silica composite and are located on the outer layer of the composite particles.

## The Buildup of Polyelectrolyte and/or Colloid Particle Multilayer on Solid Surfaces

The multilayer formation of polyelectrolytes on colloid particles is usually characterized by a stepwise increase of the adsorbed amount and layer thickness, and by alternating highly positive and negative ζ-potentials of the covered particles. Here, we describe two kinds of multicomponent layer systems using polyelectrolyte and colloid particles. One is the formation of polyelectrolyte multilayers on polymer colloids. Another is the formation of composite particles including organic and inorganic colloid particles using a layer-by-layer technique of polyelectrolytes.[35]

To emphasize the influence of the polarity of the substrate, three kinds of polystyrene lattices are employed. PS-740 lattices with large size ($2a$=740 nm) were prepared by the usual surfactant-free emulsion polymerization technique;[12] NaSS-190 lattices were made by incorporating a small amount of an ionic comonomer, sodium-*p*-vinylbenzyl-sulfate, into the polystyrene chain according to Kotera et al.[13] The charge density of NaSS-190 lattices is much higher than that of PS-740 latex. DEAM-250 lattices consist of amphoteric particles prepared by the method described by Homola and James.[36] Characteristic data for these samples are shown in Table 3. Silica samples with different particle sizes ($2a$=500, 300, and 20 nm), which were obtained from Nippon Catalisitic Co. Ltd. and Nissan Chemical Co. Ltd., were used. All these single dispersions consisted of monodisperse spherical particles with $D_w/D_n < 1.04$ always, and were used after extensive dialysis.

As the cationic polymer, poly-L-lysine (PLL-19) with a fixed molecular weight ($M$=190,000) was used, and as the anionic polymer, polystyrene sulfonate (PSSNa-50) with $M$=500,000 was used. PSSNa-50 carries a constant charge for pH 3–10. However, PLL-19 is pH-dependently charged and it is known that a fixed positive charge is carried only in the region of pH 3–7.

The adsorption of polyelectrolytes was allowed to take place for 1.5–2 hr at a 0.1–0.3 mg/mL PLL or PSSNa solution using a very dilute latex or silica suspension ($\phi$=0.0001) and a saturated concentration without any free polymer of each polyelectrolyte that was determined by mobility measurements of the core particles. During the adsorption process, suspensions of the core particles were mixed slowly by means of rotating end-over-end.

The DLS measurements were carried out to assess the development of hydrodynamic layer thickness on the addition of PLL or PSSNa molecules. The heterocoagulated state of composite particles was observed directly by the optical microscope and scanning electron microscope.

### Multilayer formation of polyelectrolytes on colloid particles

In Fig. 17, a typical cyclical curve of ζ-potential on alternating additions of PLL-19 and PSSNa-50 on negatively charged NaSS-190 latex surfaces is shown. The switch to either of the new polyelectrolytes is

**Table 3** Particle diameters, ζ-potentials, and functional groups of the colloids

| Particle | Diameter (nm) | ζ-Potential (mV) in $10^{-3}$ M NaCl | Functional group |
|---|---|---|---|
| NaSS-190 latex | 190 | − 50 (pH 4) | $SO_3^-$ |
| DEAM-250 latex | 252 | + 60 (pH 4) | $\rangle NH^+$ |
| PS-740 latex | 740 | − 30 (pH 4) | $OSO_3^-$ |
| Silica-500 | 500 | − 30 (pH 6) | $SiO_2^-$ |
| Silica-300 | 300 | − 30 (pH 6) | $SiO_2^-$ |
| Silica-20 | 20 | − 30 (pH 6) | $SiO_2^-$ |

indicated by the arrows. In the figure, the abscissa axis indicates the total number of repeating units of both polyelectrolyte molecules. The change of the $\zeta$-potential is substantial (i.e., the $\zeta$-potential is highly positive after the addition of PLL-19 and highly negative after the addition of PSSNa-50). This result indicates clearly that, on the adsorption of polyelectrolyte, the oppositely charged surface is not just compensated but strongly overcompensated. An overcompensation of polyelectrolyte adsorption is the main reason for progressing the multilayer formation. The buildup process was also confirmed from the stepwise increase of the layer thickness of the core latex particles. The stepwise increase of the layer thickness, especially after the adsorption of PSSNa-50 molecules on the core particle surfaces, is also shown in Fig. 17.

In the next stage, we tried to produce polyelectrolyte multilayers under different medium compositions. In Fig. 18, the results of multilayer formations of PSSNa-50 and PLL-19 in pure water at pH 4, $10^{-2}$ M NaCl solution, and $10^{-2}$ M $BaCl_2$ solution are indicated. In these experiments, the positively charged DEAM-250 lattices were used as the core particles. In this figure, the

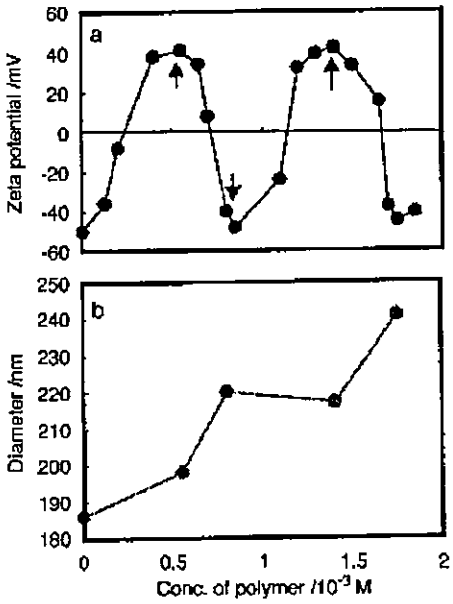


Fig. 17 $\zeta$-Potential (a) and total particle size (b) of the composite system by multilayer deposition of PLL-19 and PSSNa-50 on NaSS-10 lattices against the concentrations of each polyelectrolyte solution ($\phi$ = 7.5 × $10^{-3}$ wt.%, pH 4, [NaCl] = 1 × $10^{-3}$ M). The switch to a new polymer solution is indicated by the arrows.

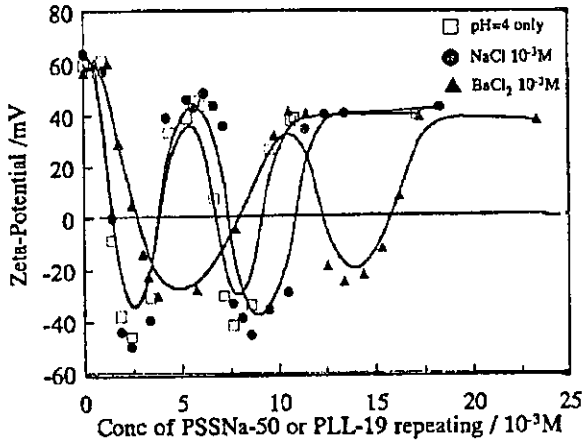


Fig. 18 $\zeta$-Potential of multilayers of PSSNa-50 and PLL-19 on DEAM-250 lattices against the concentrations of each polyelectrolyte solution under different salt conditions ($\phi$ = 7.5 × $10^{-3}$ wt.%, pH 4).

locus of $\zeta$-potentials obtained under different salt conditions is plotted for the total amounts of repeating units of PLL-19 and PSSNa-50 molecules. As can be seen, the step in the $\zeta$-potential obtained in the $BaCl_2$ solution is delayed, indicating that the electrostatic attraction between PSSNa-50 and the charged surface of DEAM-250 lattices is weakened. This is caused by the strong affinity of $Ba^{2+}$ to $SO_3^-$ in PSSNa-50 molecules. The existence of such a specific effect has been reported in the literature.[37,38]

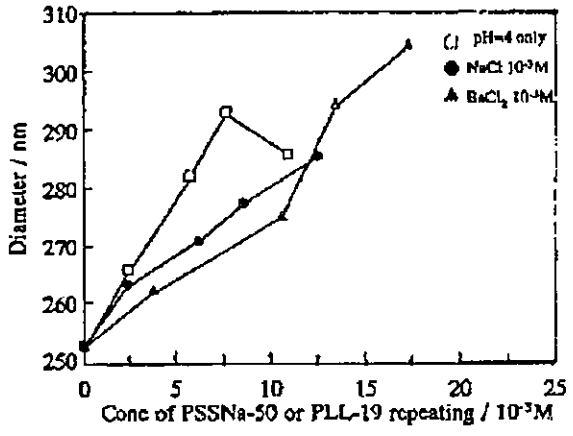


Fig. 19 The total particle sizes in each step to stable multilayers of PSSNa-50 and PLL-19 on DEAM-250 lattices under different salt conditions ($\phi$ = 7.5 × $10^{-3}$ wt.%, pH 4).

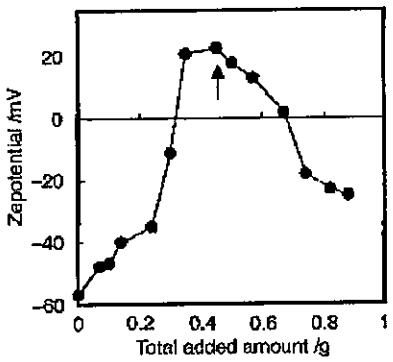


**Fig. 20** ζ-Potential of composite particles by multilayer deposition of PLL-19 (concentration, $2 \times 10^{-4}$ wt.%) and Silica-300 (concentration, $1.0 \times 10^{-3}$ wt.%) on PS-740 lattices ($=7.5 \times 10^{-4}$ wt.%, pH 6, [NaCl]$=1 \times 10^{-3}$ M). The switch to Silica-300 from PLL-19 is indicated by the arrow.

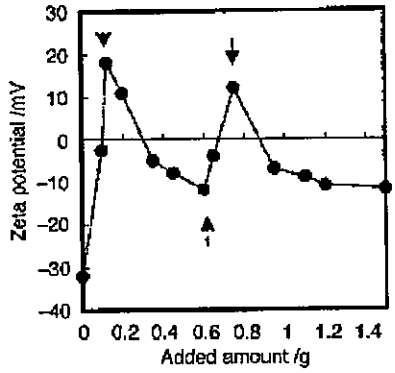


**Fig. 22** ζ-Potential of composite particles by multilayer deposition of pair (PLL-19 + Silica-20) layers. The switch is indicated by the arrow.

Fig. 19 indicates the stepwise increase of layer thickness on DEAM-250 latex particles under different salt conditions. Surprisingly, in the $10^{-2}$ M $BaCl_2$ solutions, the layer thickness of adsorbed polyelectrolytes increased steadily and the weak attraction effect coming from $Ba^{2+}$ was not observed on the layer-by-layer formation. However, in distilled water, the layer thickness increased quickly at an early stage of deposition. However, in the final stage, the layer shrunk. The reason for this phenomenon cannot be explained, but this result indicates surely that strong electrostatic attraction is not always the sole factor necessary to form a stable multilayer.

## Multilayer formation of colloid particles with polyelectrolytes

The layer-by-layer deposition technique of polyelectrolytes can be applied to the formation of composite particles comprising organic and inorganic colloid particles.

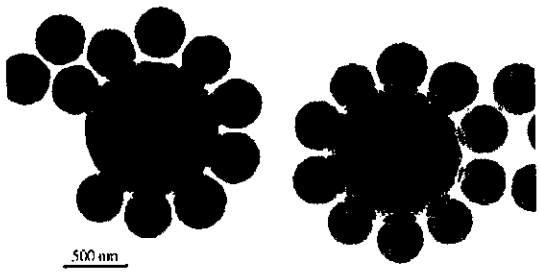


**Fig. 21** Electron micrograph showing hybrid particles of outer Silica-300 particles on core PS-740 lattices.

Fig. 20 shows the buildup processes of colloid particles using PS-740 latex sample as the core. Here, PLL-19 was used as a binder polyelectrolyte. The abscissa axis in this figures indicates the total amounts of the binder polyelectrolyte + adhering particles. As can be seen from the figure, the ζ-potential of the core particle has changed from a negative value to a positive value by adsorption of PLL-19 molecules, and changed again to negative values with an increasing number of adhering silica particles (Silica-300). These results suggest that the composite formation of colloid particles has progressed reasonably by the binder layer of PLL-19 molecules. Fig. 21 is a photograph showing a typical example of hybrid particles consisting of outer Silica-300 particles on core PS-740 latex as prepared in this experiment. It is known that the composite consists of regular hybrid particles comprising organic and inorganic particles. However, the structure form is not so stable and sometimes the system includes free silica particles.

In the next stage, the synthetic process of hybrid particles with multilayers of silica particles on PS-740 was examined. As the binder polyelectrolyte, the PLL-19 molecule was also used under the same medium conditions. Fig. 22 shows the cyclical behavior of the ζ-potential in the formation process of multilayers of Silica-20 and PLL-19 layers. As can be seen, the cycle of ζ-potential after adhesion is systematical, indicating that the deposition of PLL and Silica-20 has progressed regularly. Fig. 23 is a photograph of an original PS-740 latex and two kinds of composite particles covered with a single silica + polymer layer and two silica + polymer layers. Two kinds of composite particles can be distinguished based on the thickness of the adhering silica particle layer.


**Fig. 23** Electron micrograph showing hybrid particles of small Silica-20 particles on core PS-740 latex particles: (a) PS-740 lattices; (b) hybrid particles deposited by a single (PLL-19 + Silica-20) layer; (c) hybrid particles deposited by pair (PLL-19 + Silica-20) layers.

From these results, it is concluded that, by combining a multilayer formation of polyelectrolytes and charged colloid particles, we can prepare many new synthetic materials comprising different chemical species, different structures, and different shapes.

## CONCLUSION

Here, several preparation processes of composite particles relating to the electrical properties of particles are described: 1) the heterocoagulation process of amphoteric polymer lattices on spherical silica; 2) composite formation comprising silica/vesicle or silica/vesicle/silica particles; and 3) the buildup process of polyelectrolyte or colloid particle multilayers on latex or silica surfaces. All these results indicate that the electrokinetic measurement is an essential and powerful technique for monitoring the formation process of composite particles with different compositions. Finally, the present authors would like to stress that the formation processes described here were concerned with the semimicron-sized particles, but these techniques can be applied to systems, including nanosized particles with slight reversions.

## REFERENCES

1. Matijevic, E. *Interfacial Electrokinetics and Electrophoresis*; Delgado, A.V., Ed.; Surfactant Science Series, Marcel Dekker, Inc.: New York, 2002; Vol. 106, 199–218.
2. *Electrical Phenomena at Interfaces*; Ohshima, H., Furusawa, K., Eds.; Surfactant Science Series, Marcel Dekker, Inc.: New York, 1998; Vol. 76.
3. Lyklema, J. *Fundamentals of Interface and Colloid Science*; Academic Press, Inc.: London, 1995; Vol. II.
4. von Smoluchowski, M. *Handbuch der Electrizitat und des Magnetismus*; Graetz, W., Ed.; Barth: Leipzig, 1914; Vol. II, 366.
5. Komagata, S. Nihon Kagaku Kaishi **1932**, *53*, pp. 342, 969.
6. Furusawa, K.; Uchiyama, K. J. Colloid Interface Sci. **1998**, *140*, 217.
7. Sasaki, H.; Muramatsu, A.; Arakatsu, H.; Usui, S. J. Colloid Interface Sci. **1991**, *142*, 266.
8. Usui, S.; Imamura, Y.; Sasaki, H. J. Colloid Interface Sci. **1987**, *118*, 335.
9. Marlow, B.J.; Fairhurst, D.; Pendse, H.P. Langmuir **1988**, *4*, 611.
10. O'Brien, R.W.; Midmore, B.R.; Lamb, A.; Hunter, R.J. Faraday Discuss. Chem. Soc. (London) **1990**, *90*, 301.
11. Dukhin, A.S.; Shilov, V.N.; Oshima, H.; Goetz, P.J. Langmuir **1999**, *15*, pp. 6692, 3445.
12. Hozumi, Y.; Furusawa, K. Colloid Polym. Sci. **1990**, *268*, 469.
13. Kotera, A.; Furusawa, K.; Takeda, Y. Kolloid-Z. Z. Polym. **1970**, *239*, 677.
14. Juang, M.S.; Krieger, I.M. J. Polym. Sci. **1976**, *14*, 2089.
15. Van den Hul, H.J.; Vanderhoff, J.W. Electroanal. Chem. **1972**, *37*, 161.
16. Kolthoff, I.M.; Miller, I.K. J. Am. Chem. Soc. **1951**, *73*, 3055.
17. Ottewill, R.H.; Shaw, J.N. Kolloid-Z. Z. Polym. **1976**, *218*, 34.
18. Hearn, J.; Ottewill, R.H.; Shaw, J.N. Br. Polym. J. **1972**, *2*, 116.
19. Levine, S.; Neale, G.; Epstein, N. J. Colloid Interface Sci. **1976**, *57*, 427.
20. Greenwood, R.; Bergstrom, L. J. Eur. Ceram. Soc. **1997**, *17*, 537.
21. Furusawa, K.; Anzai, C. Colloid Polym. Sci. **1987**, *265*, 882.

22. Furusawa, K.; Kimura, Y.; Tagawa, T. J. Colloid Interface Sci. **1986**, *109*, 69.
23. Velev, O.D.; Furusawa, K.; Nagayama, K. Langmuir **1996**, *12*, pp. 2374, 2385.
24. Wilcox, D.L.; Berg, M. Hollow and Solid Spheres and Microspheres. In *Proceedings of the Materials Research Society, Pittsburgh*; Wilcox, P.L., et al., Eds.; Science and Technology Associated with Their Fabrication and Application, 1995; Vol. 372, 3–13.
25. Iler, K.K. J. Colloid Interface Sci. **1966**, *21*, 569.
26. Decher, G.; Hong, J.D. Ber. Bunsenges. Phys. Chem. **1991**, *95*, 1439.
27. Decher, G. Science **1997**, *277*, 1232.
28. Caruso, F.; Mohwald, H. Langmuir **1999**, *8276*, 15.
29. Caruso, F.; Caruso, R.A.; Mohwald, H. Science **1988**, *1111*, 282.
30. Gherardi, P.; Matijevic, E. Colloid Interface Sci. **1986**, *109*, 57.
31. Furusawa, K.; Anzai, C. Colloids Surf. **1992**, *63*, 103.
32. Furusawa, K.; Velev, O.D. Colloids Surf., A Physicochem. Eng. Asp. **1999**, *159*, 359.
33. Yang, B.; Matsumura, H.; Katoh, K.; Kise, H.; Furusawa, K. Langmuir **2001**, *17*, 2283.
34. Lehrmann, R.; Seeling, J. Biochim. Biophys. Acta **1994**, *1189*, 89.
35. Furusawa, K.; Satou, S. Colloids Surf. **2001**, *195*, 143.
36. Homola, A.; James, R.M. J. Colloid Interface Sci. **1977**, *59*, 123.
37. van Duelm, P.; Norde, W.; Lyklema, J. J. Colloid Interface Sci. **1977**, *59*, 123.
38. Furusawa, K.; Tomotsu, N. J. Colloid Interface Sci. **1983**, *93*, 504.



Marcel Dekker, Inc.
270 Madison Avenue, New York, New York 10016

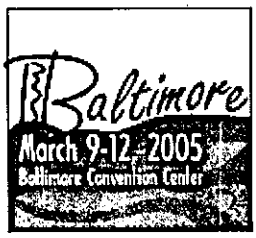


› Abstracts by Program
› Search
› Author Index
› Subject Index
› Program Book
› CD Help
› Main Menu

**ABSTRACT: 2005 IADR/AADR/CADR 83rd General Session & Exhibition**

# 2061 Clinical trials on eary caries detection using QLF technique

*M. UEMURA*, T. DOI, T. MIYAKE, Y. SAKAMOTO, and M. KAMBARA, Osaka Dental University, Japan*

Objective: The present study was clinically to determine the ability of a quantitative light-induced fluorescence (QLF) technique for detection and quantification of white spot lesion. Methods: Sixty five of white spot lesions in 65 patients (Mean age: 20.378.3) were selected by visual inspection of oral examination and then evaluated using a QLF technique. The QLF images were saved at the initial visit and were compared with images done one year later. This allows us to quantify demineralization and/or remineralization. The image of each white spot lesion was analyzed for four parameters. The average depth of the lesion was measured as the average of fluorescence loss (delta F, %). The maximum lesion depth was measured as the maximum fluorescence loss (delta Max, %) as maximum lesion depth. The lesion size (S, $mm^2$) was also analyzed from each QLF image of white spot lesion. The mineral loss (delta Q, %X$mm^2$) was calculated by the both of delta F and S for each white spot lesion. Results: All of white spot lesions detected at the initial visual inspection were judged as early caries lesion with QLF measurements (delta Q was -14.8%$mm^2$, delta F:-8.9%, delta Max:-20.5% and S:1.4 $mm^2$). The white spot lesions detected with QLF at the initial measurement progressed in 53.8% at one year later. 43.1% of the lesion regressed and 3.1% arrested at one year later. Conclusion: Based on these results, we concluded that QLF technique is suitable for early detection and assessment of dental caries clinically.

Seq #229 - Early Diagnosis Posters
2:00 PM-4:00 PM, Friday, 11 March 2005
Baltimore Convention Center Exhibit Hall E-F

Back to the Cariology Research Program
Back to the IADR/AADR/CADR 83rd General Session (March 9-12, 2005)

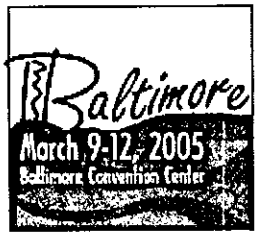


› Abstracts by Program
› Search
› Author Index
› Subject Index
› Program Book
› CD Help
› Main Menu

**ABSTRACT: 2005 IADR/AADR/CADR 83rd General Session & Exhibition**

# 2059 Evaluation of red-fluorescent dental plaque using QLF method

*K. KAWASAKI*, R. SAKAI, R. TAKASHIMA, and M. KAMBARA, Osaka Dental University, Hirakata-shi Osaka, Japan*

Objectives: We investigated the detection and analysis possibility of red-fluorescent dental plaque using quantitative light-induced fluorescence (QLF) method. Methods: The QLF (Inspektor Research Systems B. V., The Netherlands) examination of the digital image of red-fluorescent dental plaque was used to calculate the detected area (AREA), the average red-fluorescence intensity (Δ R ave.) and the maximum red-fluorescence intensity (Δ R max) in 10 healthy volunteers who refrained from tooth brushing for four days. The collected samples of red-fluorescent dental plaque were analyzed by the technique of polymerase chain reaction (PCR) for detecting periodontal disease related bacteria (*Actinobacillus actinomycetemcomitans*, *Porphyromonas gingivalis*, *Prevotella intermedia*, *Bacteroides forsythus* and *Treponema denticola*). Results: The most of red-fluorescent dental plaque were observed at buccal and lingual surfaces of molar teeth, and the lingual surface of lower anterior teeth. Each of the three QLF parameters increased at a different rate for the four days. The average value of each parameters showed a different value for every subject, and a different increasing tendency. As the result of analyzing the red-fluorescent dental plaque by the PCR method, it turns out that the periodontal disease related bacteria exists at red-fluorescent dental plaque. Conclusion: We concluded that the QLF examination can distinguish and quantify the three parameters, and evaluate the rate of dental plaque formation.

Seq #229 - Early Diagnosis Posters
2:00 PM-4:00 PM, Friday, 11 March 2005
Baltimore Convention Center Exhibit Hall E-F

Back to the Cariology Research Program
Back to the IADR/AADR/CADR 83rd General Session (March 9-12, 2005)

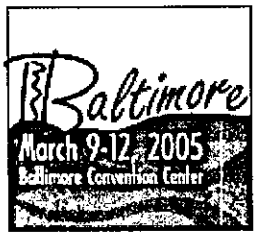


› Abstracts by Program
› Search
› Author Index
› Subject Index
› Program Book
› CD Help
› Main Menu

**ABSTRACT: 2005 IADR/AADR/CADR 83rd General Session & Exhibition**

# 2051 *In vitro* QLF observation of remineralizing effect in fluoride applications

*R. SAKAI*, R. TAKASHIMA, K. KAWASAKI, and M. KAMBARA, Osaka Dental University, Hirakata, Osaka, Japan*

Objectives: The purpose of this *in vitro* study is to evaluate the remineralizing process of incipient enamel lesions in topical fluoride applications with quantitative light-induced fluorescence (QLF). Methods: 160 bovine enamel specimens (5 mm in diameter) were mounted in acrylic rod and polished. Incipient lesions were formed in specimens by 12 to 96 hour immersion in demineralizing solution (Lactic acid: 100 mM, Hydroxiapatite: 3 g/L, Carboxymethyl cellulose sodium salt: 0.2 g, pH: 5.0). These lesions were quantitatively calculated with Δ F (% / ratio of fluorescent loss which describes lesion depth) and divided into 4 groups (Δ F = -8, -16, -24 and -32). These groups were further divided by treatment (control, Fluoride dentifrice, APF and Fluoride dentifrice + APF). Specimens were immersed in artificial saliva for 28 days (KCl: 130 mM, $KH_2PO_4$: 0.9 mM, $CaCl_2$: 1.5 mM, HEPES: 20 mM, pH: 7.0). Surface images of the remineralizing process were recorded on days 3, 6, 9, 12, 15, 21 and 28 with QLF (Inspektor Reserch Systems, The Netherlands). Results: In low demineralized groups (Δ F = -8 and -16), recovery rates reached the plateau within 6 days. In high demineralized groups (Δ F = -24 and -32), recovery rates in the two APF treated groups reached the plateau in 6 days, and in others, the rates kept raising for 2 weeks. In all lesion specimens, rates of the control and Fluoride dentifrice groups were higher than the two APF treated groups. ($p < 0.05$). There was no difference between the two APF treated groups, and neither was there between control group and Fluoride dentifrice group ($p > 0.05$). Conclusion: This *in vitro* study showed that the difference in recovery rates among 4 types of fluoride treatment could be observed using QLF. This suggests the usefulness of QLF in clinical applications.

Seq #229 - Early Diagnosis Posters
2:00 PM-4:00 PM, Friday, 11 March 2005
Baltimore Convention Center Exhibit Hall E-F

Back to the Cariology Research Program
Back to the IADR/AADR/CADR 83rd General Session (March 9-12, 2005)

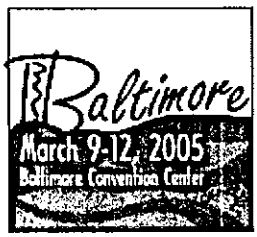


› Abstracts by Program
› Search
› Author Index
› Subject Index
› Program Book
› CD Help
› Main Menu

**ABSTRACT: 2005 IADR/AADR/CADR 83rd General Session & Exhibition**

# 1069 New Analysis Method of Gingiva with Quantitative Light-Induced Fluorescence

*M. IZU*, T. MIYAKE, M. UENE, H. TANAKA, R. TAKASHIMA, N. NISHIJIMA, and M. KAMBARA, Osaka Dental University, Japan*

Objectives:The purpose of this study was to evaluate the condition of gingiva objectively by a new digital image analysis with Quantitative Light-Induced Fluorescence (QLF).

Methods:15 adults (mean age; 22-26 years old) who were informed about the aim of this study and agreed to participate, were selected as the subjects. Photographs of the gingiva were taken with an oral CCD camera (COREFRONT CORPORATION, Tokyo, Japan) and INSPEKTOR PRO(Inspektor Research Systems B.V., Amsterdam, The Netherlands). Subjects were prohibited blushing for 7 days. They were re-examined by same methods after 1, 2, 3, 5 and 7 days. The condition of gingiva was analyzed from the digital images obtained from INSPEKTOR PRO by a computer program (Inspektor-Pro 1.2.0.4, Inspektor Research Systems B.V., Amsterdam, The Netherlands).

Results:On inspection, changes in the gingiva after each day could hardly be observed. However, when analyzing the images of gingiva, it was observed that a change in the color tone of the gingiva was more objectively expressed with red in the gingiva over green in the teeth fluorescence radiance that on the reference point increase, and the change of their gingival inflammation was to quantitatify with this parameter in %.

Conclusions:As a result of analyzing the digital images of gingiva by QLF, it was suggested that this newly developed analyzing method could be useful for gingival examination, as changes in the quantitative value expressed the condition of the gingiva.

Seq #127 - Diagnosis, Aggressive Periodontitis, Clinical States
2:00 PM-4:00 PM, Thursday, 10 March 2005
Baltimore Convention Center Exhibit Hall E-F

Back to the Periodontal Research - Diagnosis / Epidemiology Program
Back to the IADR/AADR/CADR 83rd General Session (March 9-12, 2005)

# QLF (Qualitative Light-induced Fluorescence) による齲蝕診断

神原　正樹
大阪歯科大学口腔衛生学講座

2005年37巻3月増大号（通巻480号）
細胞（p.6～p.9）
ニューサイエンス社

# 【QLF (Qualitative Light-induced Fluorescence) による齲蝕診断】

Early Detection of Incipient Caries Using QLF

神原　正樹

Kambara　Masaki

Key words
Incipient caries, Detection, Diagnosis, QLF

## Abstract

初期齲蝕（白斑，可逆的齲蝕，表層下脱灰）の段階で齲蝕を検出し，画像処理により定量化することが可能な新たな技術が出現してきているが，その中に，優れた特徴を有する光誘導蛍光定量法（QLF法，Quantitative Light-induced Fluorescence）がある。ある波長の光を歯に照射するとエナメル質と象牙質の境界部に存在する蛍光物質が励起され，反射するが，初期齲蝕部では乱反射し，黒色を呈するというQLF法の原理を解説するとともに，歯科医療における初期齲蝕早期検出の意味（齲蝕臨床の科学的裏づけ，齲蝕窩洞の定量化，画像取得，初期齲蝕評価，インフォームド・コンセントの確立）やQLF法の応用例（*in vitro*，clinical study，臨床応用）を紹介する。

## はじめに

21世紀の歯科医療が住民主体の歯科疾患予防や口腔の健康増進に向かっている。これは，齲蝕が顕著に減少し，目に見えない歯科疾患が増加し，これまでの歯科領域になかった住民の歯科に対する需要が増加していることによる。この口腔疾患の予防や健康増進のための新たな歯科医療を構築することが，歯科医学に突きつけられた急を要する課題である。その中で，齲蝕に対するEvidence-basedな技術が出現し始めており，リスク管理としての齲蝕検査システムや早期齲蝕検出が注目を集めている[1,2]。

## 1．早期齲蝕検出の意味

予防や健康増進のための歯科医療は，齲蝕に対しては，できるだけ早期に検出し，現在行われているような歯を切削して充填することなく予防処置で回復さすことを目指すことになる。予防処置による回復は，齲蝕の早期段階であれば，フッ化物による再石灰化の生ずることが明らかにされており，これを利用することになる。齲蝕の早期段階，すなわち初期齲蝕とは，臨床的には白斑として認識されており，組織学的には表層下脱灰像を呈する可逆的齲蝕を意味する（図1）。すなわち，X線による診査では検出しえない初期齲蝕を検出し，予防処置を行うなど，健全歯の管理を行うことになる。このことは，Caries prevention is invisible（齲蝕予防は見えない）からCaries prevention is visible（齲蝕予防が見える）への変遷を行うことになり，このことが早期齲蝕検出の必要性の意味である。この背景には，歯の自然史（萌出した健全歯が，充填を繰り返し，歯冠修復が行われ，喪失してしまう歯の顛末）のエビデンスやこれに対する反省，健全歯の増加，国民の健康志向の上昇，新たな歯科医療の模索，歯科医学の進展などがあり，健全歯の質的評価や初期齲蝕の検出などの課題解決が望まれていることがある。

齲蝕リスク診断は，齲蝕発病の危険度を診査することであるが，病原因子，環境因子，生活習慣因子，すなわち齲蝕侵襲因子のみに限られているのが現状であり，宿主要因についてのリスク分析ができていない。そのため，今後の歯科医療，健康な歯をどのように維持・管理していくかとの視点では，歯のリスク要因の客観的評価が行えるようにすることが必要である。

大阪歯科大学口腔衛生学講座：Department of Preventive and Community Dentistry, Osaka Dental University
〒573-1121　大阪府枚方市楠葉花園町8-1　Fax: 072-864-3119　E-mail: kambara@cc.osaka-dent.ac.jp

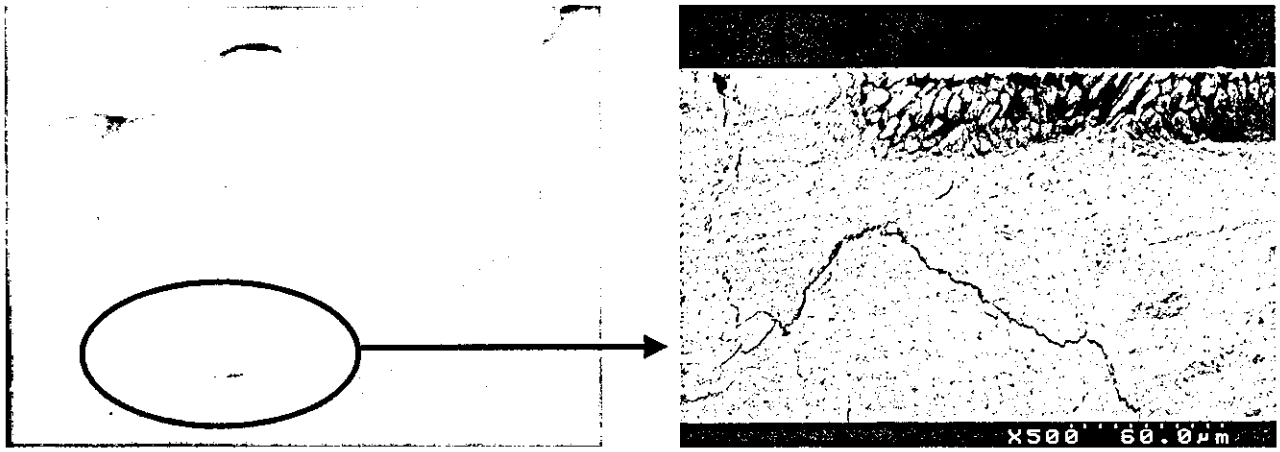


白斑　　表層下脱灰像

図1　初期齲蝕（白斑）の臨床像と組織像

健全歯のリスク評価は，歯の形態評価（小窩裂溝の複雑性，深さ，色等），歯の質的評価（フッ化物含有量，抵抗性等）などの客観的評価法を確立することが必要である。ついで，初期齲蝕（予防処置で回復可能な表層下脱灰；incipient or early caries, white spot）のAssessment of incipient caries（初期齲蝕評価），すなわち初期齲蝕検出後の初期齲蝕の特性あるいは監視を行うとの目的に沿った以下の評価が出来るようにするべきである。①Progression of Caries（齲蝕進行性：深部に拡がろうしている状態にある齲蝕），②Arrestment of Caries（齲蝕停止性：進行せず，回復もしない安定状態にある齲蝕），③Regression of Caries（齲蝕回復性：健全に戻ろうとしている齲蝕）。

## 2．早期齲蝕診断法（QLF法）

早期齲蝕診断法としては，その具備条件に，非侵襲性であることはもちろんであるが，TMRなどのエナメル質内部での表層下脱灰との相関性，再現性や，脱灰状態の定量化，さらには画像表示が出来ることなどが早期齲蝕検出法に要求されている。現在開発をされている，あるいは商品化された早期齲蝕検出技術には，レーザーを照射し，齲蝕窩洞内の細菌産生の蛍光物質を検出する方法，歯の電気抵抗性の変化を測定する方法，歯の透過光による影を観察する方法，光誘導蛍光定量法などがある。個々技術の検出原理は異なるが，長年にわたり研究されてきた継続性が今日の使用できる技術となって実を結んできている。

その中で，唯一初期齲蝕の定量化が可能なのがQLF法である。光誘発蛍光定量法(QLF; Quantitative Light-induced Fluorescence)は，光照射することにより歯のエナメル質と象牙質境界部に存在する蛍光を励起し，反射する蛍光が表層下脱灰部において乱反射することにより黒色を呈する。この画像をフィルターを通してCCDカメラでコンピュータに取り込み，取り込んだ画像を画像解析し（健全エナメル質との比較で判断し，脱灰面積，最大深さ，平均深さ，脱灰量として数値化），脱灰部の定量化を図るものである（図2）。歯が蛍光を有していることは，歴史的に古くから知られており，1926年Benedict[3]が，エナメル質，象牙質の蛍光を可視，紫外線(UV)範囲で励起できることを初めて示したとされている。それ以来，多数の研究者により研究されてきているが蛍光物質の特定にはいまだいたっていない。1963年Armstrong[4]は象牙質の蛍光は各種無機物質と有機物質の複合体であると示唆し，1980年Foteman[5]は象牙質の蛍光物質がアミノ酸tryptophanと未知物質であると報告し，1976年Spitzer & ten Bosh[6]はエナメル質の蛍光物質は有機物質であるなどの報告があるが，有機物であるらしいとの認識段階である。

QLF法が他の早期齲蝕検出法とは異なる特徴を有しているのは，初期齲蝕の定量化（齲蝕面積，脱灰深さならびに脱灰量）および初期齲蝕脱灰の画像化である。QLF法により，実用化に向けて，QLF法の有用性について研究を進めている段階であるが，我々の講座で得られた興味深い結果を以下に示す。

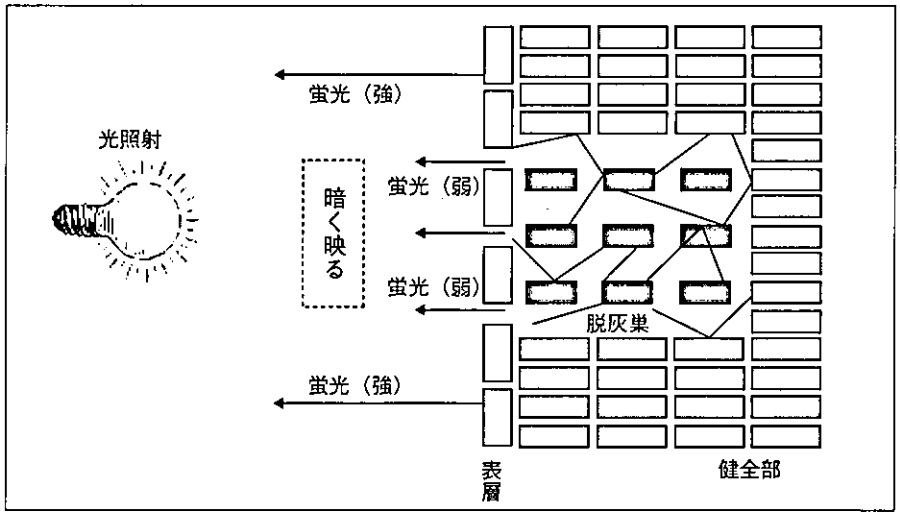


図2　QLF法 初期齲蝕検出原理

1）*in vitro*研究

フッ化物による人工的初期齲蝕再石灰化のQLFによる実験では，初期齲蝕の窩洞が小さいものの方が再石灰化は100%に近いところまで起こるが，初期窩洞が大きいと再石灰化は完全には元に戻らない。フッ化物の濃度が高いと，再石灰化は元に戻らないなど，再石灰化は条件により異なることが明らかになってきている。初期齲蝕の程度に応じ，どの条件で再石灰化が最も起こりやすいか等，フッ化物の効果的応用方法の解明の可能性が広がったと考えている。

2）臨床研究

QLF法を用いたフッ化物配合歯磨剤の臨床研究（1年間）の結果を示す。コントロールであるフッ化物非配合歯磨剤使用の初期齲蝕における1年後の結果は，齲蝕が進行した初期齲蝕は53.8%，齲蝕が回復（再石灰化）した初期齲蝕43.1%であった。回復（再石灰化）をする初期齲蝕が半数見られること，口腔内での人間の自然回復能には驚きを覚える。一方，ある種のフッ化物配合歯磨剤を指示した初期齲蝕は，1年後87.5%の回復を示した[7-10]。これまで報告されてきたフッ化物配合歯磨剤の齲蝕抑制効果は，30-40%程度であった結果と比較すると非常に高い齲蝕抑制率である。齲蝕検出を視診で行ってきた方法とQLF法の定量化による齲蝕検出との精度の違いを示したものと考えられる。

3）臨床応用

QLFでの臨床応用した例を図3に示す。3歯の初期齲蝕を1週ごとに3回観察した結果であるが，上段と下段の初期齲蝕画像に変化は見られず，停滞性の齲蝕であると評価できる。一方，中段の初期齲蝕は拡大傾向にあり，進行性齲蝕であると評価できる。このように，間隔をあけて初期齲蝕を観察することにより，初期齲蝕の定量的に評価（進行性，停滞性，回復性）をすることができ，しかもこの結果を画像として示すことが可能である。画像での表示は，患者とのインフォームドコンセントの取得に有用であり，歯科治療に科学的裏づけを与えることになる。

## まとめ

齲蝕予防を実践するための技術，早期齲蝕検出法が完成すると，初期齲蝕の評価（進行・停止・回復）ができ，各歯に応じたテーラーメイド齲蝕予防治療が可能になる。また，現在行われている環境要因を中心とした齲蝕リスク評価にホスト要因を加えることができ，より，精度の高い齲蝕リスク評価を行うことができるようになる。さらに，齲蝕治療（充填処置，補綴処置）の二次齲蝕発現の有効性評価や新たな予防処置・剤の開発にもつながる可能性がある。

このように，早期齲蝕検出法が確立されようとしている現在，初期齲蝕検出後の新たな予防処置システムの確立が望まれる。さらに，早期齲蝕検出法は，歯の健康を獲得するための各種方面に影響を及ぼす可能性を持っており，歯科医療がEvidence Basedな健康保持増進・予防へ転換するきっかけになることを信じてやまない。

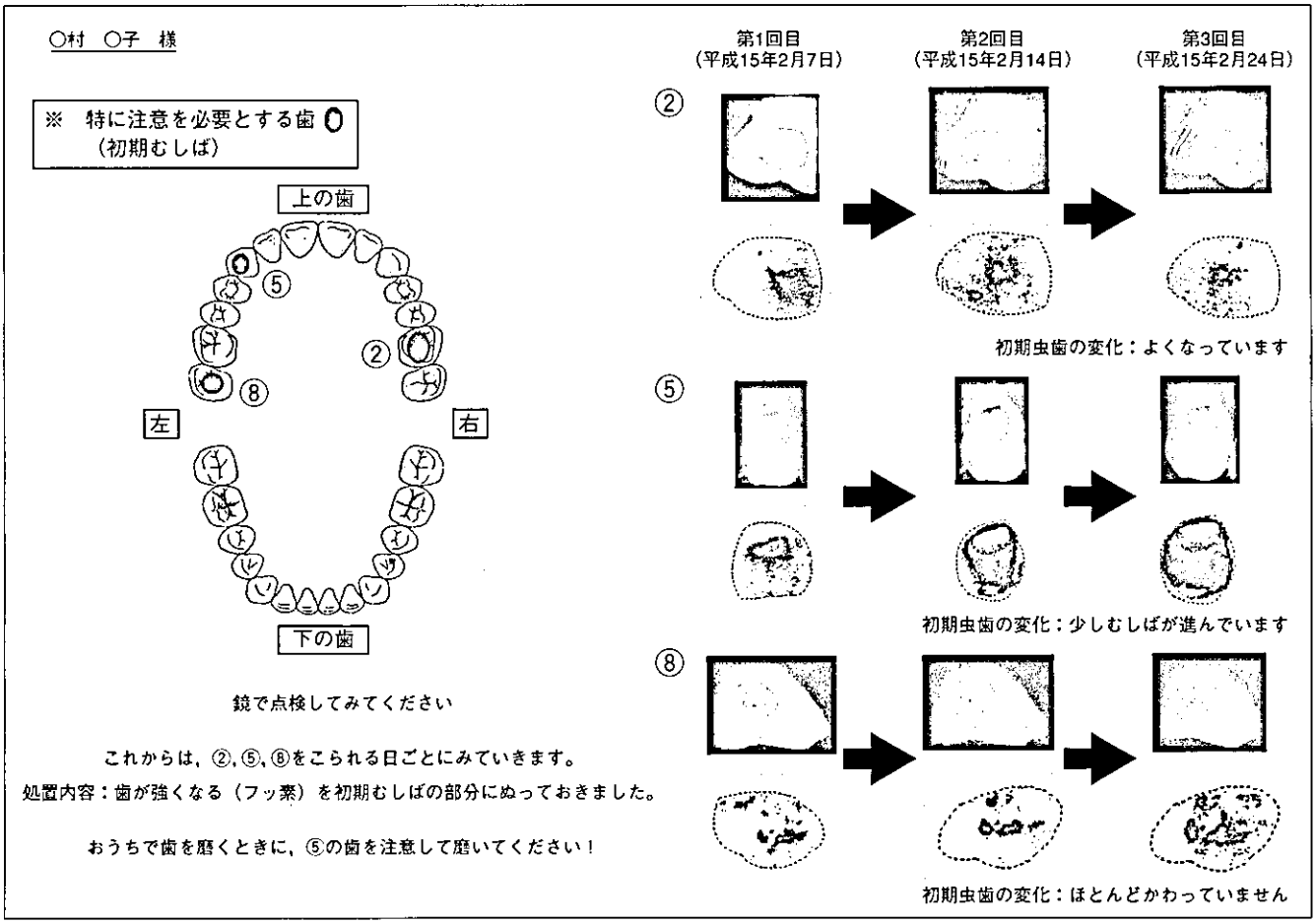


図3　QLF法の臨床応用例（ある患者の3回取得したQLF画像）

## 文　献


1) 神原正樹.: 予防歯科へのストラテジー －齲蝕予防における早期齲蝕診断－. 日本歯科医師会雑誌. 56: 611-618, 2004.
2) Early Detection of Dental Caries II, Edited by G.K. Stookey, Proceedings of the 4th Annual Indiana Conference, Indiana University School of Dentistry, 2000.
3) H C Benedict.: Note on the fluorescence of teeth in ultra-violet rays. Science. 67: 442, 1928.
4) W G Armstrong.: Fluorescence characteristics of sound and carious human dentine preparations: Arch Oral Biol. 8: 79-90, 1963.
5) P C Foreman.: The excitation of emission spectra of fluorescent components of human dentine. Arch Oral Biol. 25: 641-647, 1980.
6) D Spitzer, J J ten Bosch.: The total Luminescence of bovine and human dental enamel. Calcif Tissue Res. 20: 201-208, 1976.
7) 上村参生, 神原正樹.: 早期齲蝕診断への機器応用の必要性. The Nippon Dental Review. 63: 161-165, 2003.
8) M. Uemura, M. Kambara。 Results of clinical trials of fluoride dentifrices using quantitative light fluorescence; Early Detection of Dental Caries III, Indiana Conference, 2003.
9) 坂本吉史, 上村参生, 神原正樹.: *In vivo*におけるQLFによる早期齲蝕診断に関する研究 －初期齲蝕病巣の定量評価について－. 歯科医学. 67: 257-265, 2004.
10) 大塚秀人, 三宅達郎, 神原正樹.: *In vivo*におけるQLFによる早期齲蝕診断に関する研究 －初期齲蝕病巣の1年間の追跡結果について－. 歯科医学. 67: 266-273, 2004.


■表紙写真の解説■

定量的光誘導蛍光法（QLF法）により撮影した口腔内の天然歯。歯全体に象牙質から発せられる緑色の蛍光が観察される。歯頸部にみられる黒い影が初期齲蝕像である。初期齲蝕は肉眼で観察するのは困難であるが，QLF法による光学的診査により明瞭に初期齲蝕の検出および画像処理による定量的評価を行うことができる。

（表紙写真の提供・解説：神原 正樹）